Catalysis Today 418 (2023) 114042

Contents lists available at ScienceDirect

Catalysis Today

journal homepage: www.elsevier.com/locate/cattod

Carbon nitride – PVDF photocatalytic membranes for visible-light degradation of venlafaxine as emerging water micropollutant

Laura Valenzuela [a,*], Marta Pedrosa [b,c], Ana Bahamonde [d], Roberto Rosal [a], André Torres-Pinto [b,c], Cláudia G. Silva [b,c], Joaquim L. Faria [b,c], Adrián M.T. Silva [b,c,**]

[a] Department of Chemical Engineering, Universidad de Alcalá, Alcalá de Henares, Madrid 28805, Spain
[b] LSRE-LCM – Laboratory of Separation and Reaction Engineering - Laboratory of Catalysis and Materials, Faculty of Engineering, University of Porto, Rua Dr. Roberto Frias, 4200-465 Porto, Portugal
[c] ALiCE – Associate Laboratory in Chemical Engineering, Faculty of Engineering, University of Porto, Rua Dr. Roberto Frias, 4200-465 Porto, Portugal
[d] Instituto de Catálisis y Petroleoquímica, ICP-CSIC, Marie Curie 2, Madrid 28049, Spain

ARTICLE INFO

Keywords:
G-C_3N_4 membrane
Metal-free catalyst
Photocatalytic filtration
Contaminants of emerging concern
Continuous operation

ABSTRACT

Metal-free carbon nitride-based membranes were prepared by embedding bulk or exfoliated graphitic carbon nitride (g-C_3N_4) photocatalysts in a polyvinylidene fluoride (PVDF) matrix. Supported membranes were also fabricated by immobilising these photocatalysts on a polytetrafluoroethylene (PTFE) substrate. The membranes were tested for venlafaxine (VFX) degradation at a feed concentration of 250 μg L^{-1} under continuous flow mode operation and using a visible-light emitting diode (LED) as energy source. The reduction of the (002) diffraction peak and the increased intensity of the infrared absorption bands confirmed that the exfoliation process decreased the number of aligned g-C_3N_4 layers, with a more ordered packing of tri-s-triazine units. Additionally, the small particle size (around 745 and 257 nm for bulk and exfoliated g-C_3N_4, respectively) and the presence of terminal amino groups in the catalysts allowed for homogeneous dispersion in the PVDF matrix. Despite their different surface roughness and cross-sectional microstructure, all the fabricated membranes exhibited similar photocatalytic filtration performance for VFX degradation, resulting in conversions above 95% after 5 h of irradiation (418 nm with an irradiance of 11.2 W m^{-2}) and keeping the VFX concentration in the effluent negligible up to 48 h of continuous operation (mass removal rate of about 6 mg m^{-2} h^{-1}). In a more complex water matrix (*i.e.*, surface water), the photocatalytic filtration process led to 50% VFX removal (or 3 mg m^{-2} h^{-1}) at the steady state. Moreover, the permeate flux remained at about 25 L m^{-2} h^{-1} throughout the continuous operation, suggesting that fouling did not occur at these conditions.

1. Introduction

Organic micropollutants (*e.g.*, pharmaceuticals, pesticides, personal care products, industrial chemicals, among others) at trace concentrations (ng L^{-1} to μg L^{-1}) have been considered a threat to the environment and human health, some exhibiting ecotoxicity, endocrine interference and developing antimicrobial resistance [1–3]. Antidepressants are used for the long-term cure of depression, and for treating other health conditions, such as anxiety, panic, sleep and eating disorders, hyperactivity, and chronic pain. These substances are among the most toxic pharmaceuticals to aquatic organisms [4–6]. In particular, venlafaxine (VFX) is one of the most widely prescribed selective serotonin/norepinephrine reuptake inhibitors (SNRIs) worldwide to treat depression and generalised anxiety disorders, and its presence in the inlet of urban wastewater treatment plants (WWTPs) has been already reported [7]. Unfortunately, the physicochemical and biological treatments conventionally applied in WWTPs achieve low removal efficiencies of VFX (≈ 40%), resulting in the discharge of VFX into surface waters, where this compound might persist [8,9]. Hence, developing efficient treatment strategies is essential to effectively remove VFX and many other pharmaceutical substances from urban wastewater, and also from surface waters such as those supplying drinking water treatment

* Corresponding author.
** Corresponding author at: LSRE-LCM – Laboratory of Separation and Reaction Engineering - Laboratory of Catalysis and Materials, Faculty of Engineering, University of Porto, Rua Dr. Roberto Frias, 4200-465 Porto, Portugal.
E-mail addresses: laura.valenzuela@uah.es (L. Valenzuela), adrian@fe.up.pt (A.M.T. Silva).

https://doi.org/10.1016/j.cattod.2023.114042
Received 8 December 2022; Received in revised form 7 February 2023; Accepted 15 February 2023
Available online 16 February 2023

plants (DWTPs). In this context, heterogeneous photocatalysis is a possible treatment technology to remove these organic micropollutants in WWTPs and DWTPs, due to its cost-effectiveness, high oxidation capacity and sustainability [10,11].

Two-dimensional (2D) carbon-based photocatalysts have numerous advantages compared to the commonly used metal oxide semiconductors (*e.g.*, titanium dioxide or zinc oxide) for water and wastewater treatment. Some benefits are the larger surface area, superior optoelectronic properties, and thermal and chemical stability, while avoiding possible secondary pollution by metal leaching [12,13]. Specifically, graphitic carbon nitride (g-C_3N_4) is composed of stable tri-s-triazine networks. It has gained great interest in research owing to its simple synthesis method from earth-abundant elements and visible-light absorption, with a band gap energy of approximately 2.7 eV and suitable band positions [14,15], enabling solar-driven photocatalysis. Moreover, g-C_3N_4 allows the formation of hydroxyl radicals ($HO^{\bullet}$) and hydrogen peroxide (H_2O_2) under oxygenated conditions, which are major player species in the abatement of organic pollutants [15,16]. Low-cost light-emitting diodes (LEDs) can also be employed as visible-light sources to photoactivate g-C_3N_4, offering the possibility of designing more compact photoreactors with reduced power consumption and longer lifespan [17,18]. Despite these advantages, the practical application of pristine g-C_3N_4 is restricted by the fast recombination of photogenerated electron-hole pairs and its relatively low surface area [15,19]. Multiple approaches, including morphology control, exfoliation treatments, element doping or heterojunction design, have been applied to overcome these limitations and, thus, improve the photocatalytic performance of this material [3,20]. Among them, thermal exfoliation into 2D nanosheets stands out for its simplicity. It has been shown not only to increase the availability of active sites, promoting faster degradation of pollutants and higher H_2O_2 generation, but also to enhance g-C_3N_4 dispersibility in the preparation of materials [19,21–23].

Photocatalytic filtration combines simple physical separation and chemical oxidation processes under light irradiation in a single membrane unit. Integrating photocatalysis with membrane technologies provides a synergistic strategy to remove target pollutants from contaminated waters, solving the challenge of catalyst recovery and recycling associated with slurry reactions (usually requiring high energy-consuming processes) and allowing operation in continuous flow mode. Moreover, the presence of the photocatalyst can effectively prevent membrane fouling, which could lead to decreased flux and increased transmembrane pressure [24–30]. Photocatalytic filtration is therefore considered a green technology for environmental restoration and a potential solution to the growing energy demand, as it gives the opportunity to use renewable solar energy or LEDs, and operate under mild conditions without the addition of chemical oxidants [31].

Photocatalytic membranes can be fabricated by immobilising the catalyst on the membrane surface or by embedding it in the polymeric matrix. Supported membranes, prepared mainly through a facile vacuum filtration procedure, have demonstrated high performance but low mechanical strength owing to the poor adhesion between the catalyst and the support [32,33]. Conversely, composite membranes, in which the catalyst is blended into the polymeric matrix during the fabrication process, exhibit superior mechanical properties; however, in some cases, this strategy results in a reduction of the photocatalytic activity, as part of the catalyst is buried within the polymeric matrix [24,27]. Moreover, catalyst aggregation due to the incompatibility of g-C_3N_4 with the polymeric matrix is still a limiting factor in obtaining efficient composite membranes [32,34]. Regarding the possible polymers available for photocatalytic applications, polyvinylidene fluoride (PVDF) and polytetrafluoroethylene (PTFE) are preferred because of their high mechanical stability and resistance to ultraviolet radiation [35].

In this work, the photocatalytic filtration performance of membranes prepared with bulk or exfoliated g-C_3N_4 photocatalysts, embedded in a PVDF matrix or supported on a commercial PTFE substrate, was compared for the first time under the same experimental conditions. The antidepressant VFX was chosen as the model compound for the simultaneous photocatalytic and membrane filtration processes in continuous flow mode operation using a LED emitting at 418 nm (11.2 W m^{-2}). VFX is a contaminant of emerging concern (CEC) included in the current Watch List of 19 substances/groups of substances for European Union-wide monitoring in the field of water policy, which was published in Decision 2022/1307 [36]. The stability of the membranes was assessed by conducting long-term adsorption and photocatalytic reactions in continuous flow mode (up to 48 h). Furthermore, some VFX degradation experiments were carried out using spiked surface water (SW), approaching more realistic conditions. This study demonstrates the potential of g-C_3N_4 for application in metal-free photocatalytic membranes.

2. Materials and methods

2.1. Chemicals and water matrices

Urea (≥99.3 wt%) was obtained from Alfa Aesar (USA). Polyvinylidene fluoride (PVDF; M_W: 275,000 g mol^{-1}), polyvinylpyrrolidone (PVP; M_W: 40,000 g mol^{-1}), 1-methyl-2-pyrrolidone (NMP; 99.5 wt%) and venlafaxine hydrochloride (VFX; >98 wt%) were supplied by Sigma-Aldrich (Steinheim, Germany). For high-performance liquid chromatography (HPLC), acetonitrile (HPLC grade) and formic acid (99 wt%) were acquired from VWR (USA). All chemicals were used without further purification. Solutions containing 250 μg L^{-1} VFX were prepared in (i) ultrapure water (pH = 6.5) produced in a Milli-Q® water purification system (Merck, Darmstadt, Germany) and (ii) surface water (SW; pH *ca.* 6–7) collected from Lima River (located in the Northwestern region of Portugal). SW was stored at 4 °C and decanted for 2 h before use to remove larger suspended solids.

2.2. Synthesis and characterisation of g-C_3N_4 catalyst powders

The synthesis of bulk g-C_3N_4 was performed by thermal decomposition of urea in a Phoenix Microwave Muffle Furnace (CEM Corporation), according to a previously reported procedure [37]. Briefly, urea was placed in semi-closed quartz crucibles and underwent microwave heating (2 °C min^{-1}) up to 417 °C, remaining for 30 min, and then up to 526 °C, resting at this temperature for 1 h. The obtained powder was washed, filtered and grounded, yielding bulk g-C_3N_4. Exfoliated g-C_3N_4 was prepared by calcining the bulk material in a microwave muffle at 500 °C for 2 h. The morphology of the as-prepared photocatalytic materials was investigated by transmission electron microscopy (TEM/-STEM, JEOL 2100 F) operating at 200 kV. Additional characterisation of the bulk and exfoliated g-C_3N_4 materials is shown in our previous work [37].

2.3. Fabrication and characterisation of photocatalytic membranes

Supported photocatalytic membranes were prepared by simple vacuum filtration. To that end, 50 mg of g-C_3N_4 was added to 100 mL of ultrapure water and sonicated for 50 min to obtain a uniformly dispersed solution. The resulting dispersion was centrifuged (3500 rpm, 15 min), and the supernatant was vacuum filtered into Millipore JGWP PTFE membranes (0.2 μm pore size; 2.1 cm^2 of effective irradiated area – diameter of 1.64 cm). The remaining dispersion was dried at 100 °C overnight and weighted to determine (by mass balance) the concentration of the vacuum-filtered supernatant. The catalyst surface density of the supported membranes was set to 0.2 mg cm^{-2} by adjusting the volume of the dispersion filtered by vacuum. Dynamic particle size and surface charge (ζ-potential) of the catalyst dispersion were measured by dynamic light scattering (DLS) at 25 °C using a Zetasizer Nano ZS Instrument (Malvern).

Polymeric PVDF membranes were fabricated by the phase inversion

technique using PVP as the porogen agent and NMP as the solvent, according to a procedure described elsewhere [38]. Firstly, 0.3 g of g-C_3N_4 catalyst and 0.06 g of PVP were dispersed in 5.04 mL of NMP using an ultrasonic bath for 3 h. Then, 0.9 g of PVDF was added to the mixture, which was stirred at 40 °C for 48 h to polymerise. The resulting polymeric solution was kept stagnant overnight at room temperature to remove air bubbles. Finally, the degassed solution was spread on a glass plate using a casting knife (Elcometer 3580, Warren, MI) with a thickness of approximately 0.50 mm and immediately immersed in distilled water for a few seconds for phase inversion. The as-prepared composite membrane was stored in distilled water at room temperature until use. A reference PVDF membrane (*i.e.*, without photocatalyst) was also fabricated following the same procedure.

The crystallinity of g-C_3N_4 catalysts and g-C_3N_4-PVDF membranes was assessed by X-ray diffraction (XRD, PANalytical X'Pert Pro) using CuKα radiation. A Fourier transform infrared spectrometer (JASCO FT/IR-6800) equipped with an attenuated total reflectance (ATR) MIRacle™ Single Reflection sampling accessory (ZnSe crystal plate) was used to characterise the functional groups of g-C_3N_4 photocatalysts and g-C_3N_4-PVDF membranes in the 4000–700 cm^{-1} range. The morphology and thickness of the fabricated membranes were investigated by scanning electron microscopy (SEM, JEOL JSM-IT500 InTouchScope™) at an accelerating voltage of 15 kV after gold coating. The wettability of the membranes was evaluated by measuring the water contact angles (WCA) using the sessile drop technique (Attension Theta optical tensiometer) for five independent measurements [39].

2.4. Photocatalytic filtration experiments and analytical procedures

The membrane filtration and photocatalytic experiments were carried out in the dead-end filtration system schematically shown in Fig. 1. Briefly, the 250 μg L^{-1} VFX solution (pH of 6.2 or 7.5, respectively for ultrapure water or SW) was continuously pumped into the membrane reactor cell (working volume: 9 mL; 4.5 mL in each side of the cell) using a peristaltic pump set at a flow rate of 0.1 mL min^{-1}. This cell was irradiated using a 10 W LED emitting at 418 nm (with an irradiance of 11.2 W m^{-2} measured on the position of the membrane, and through the glass wall of the cell, with an Ocean Optics USB2000+ UV–vis spectroradiometer). Samples were withdrawn regularly from the reactor. As mentioned above, the effective membrane area was 2.1 cm^2. For comparison purposes, adsorption experiments (without irradiation) and photolytic (without membrane) runs were also performed.

The VFX concentration was determined by ultra-high performance liquid chromatography (UHPLC) using a Shimadzu apparatus equipped with an autosampler (SIL-30AC), degasser (DGU-20A5), oven (CTO-20AC), two pumps (LC-30 CE), fluorescence detector (RF-20AXS), and system controller (CBM-20 A Lite). The analysis was conducted at 30 °C using a Kinetex™ XB-C18 100 Å column (200 × 2.1 mm i.d.; particle size of 1.7 μm) provided by Phenomenex Inc. The mobile phase consisted of 0.1% (v/v) formic acid and acetonitrile under gradient mode at a flow rate of 0.25 mL min^{-1}, and the excitation/emission wavelengths were 230/300 nm.

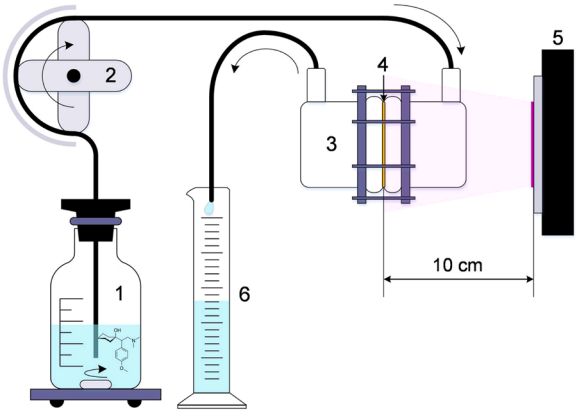

Fig. 1. Schematic representation of the dead-end filtration system: (1) feed solution bottle (250 μg L^{-1} VFX), (2) peristaltic pump (flow rate: 0.1 mL min^{-1}), (3) membrane cell (total working volume: 9 mL), (4) g-C_3N_4-based membrane (effective area: 2.1 cm^2), (5) 418 nm light source (irradiance: 11.2 W m^{-2}), and (6) permeate bottle.

Permeate flux (J_W, L m^{-2} h^{-1}) was determined through Eq. (1), where V, S and Δt denote permeated volume (L), effective membrane area (m^2) and permeation time interval (h), respectively. VFX mass removal rate ($VFX_{Removal}$, mg m^{-2} h^{-1}) was calculated by applying Eq. (2), where $[VFX]_{Influent}$ and $[VFX]_{Effluent}$ refer to the VFX concentrations in the influent and effluent of the membrane reactor (mg L^{-1}), respectively.

$$J_W = \frac{V}{S \times \Delta t} \quad (1)$$

$$VFX_{Removal} = J_W \times \left([VFX]_{Influent} - [VFX]_{Effluent}\right) \quad (2)$$

Short (2.5 h) quenching experiments were conducted to determine the main active species involved in the photocatalytic degradation of VFX. To that end, 3 mM of *p*-benzoquinone (*p*-BQ), methanol (MeOH), disodium ethylenediaminetetraacetate (EDTA) and sodium azide (NaN_3) were added to the VFX solution in ultrapure water to scavenge superoxide ($O_2^{\bullet-}$), hydroxyl ($HO^{\bullet}$), photogenerated holes and singlet oxygen ($^1O_2$) species, respectively. The pH of the scavenger solutions was adjusted to 6.2 before the photocatalytic filtration tests.

3. Results and discussion

3.1. Characterisation of the g-C_3N_4 materials

Bulk and exfoliated g-C_3N_4 powders were characterised by TEM (Fig. 2). 2D single-layered, mostly overlapping, g-C_3N_4 sheets were observed for both bulk and exfoliated materials, displaying remarkable morphological differences. Bulk g-C_3N_4 exhibited a spongy layered structure with uniformly distributed pores ranging from 10 to 60 nm in diameter (Fig. 2a, c and e). On the other hand, the exfoliated material displayed a strongly wrinkled structure with sharpened sheets and missing pores (Fig. 2b, d and f). The g-C_3N_4 photocatalytic powders were already characterised in our previous study by other techniques [37]. As shown therein, these morphological features resulted in an extraordinary increase in pore volume and surface area from 135 cm^3 mg^{-1} and 36 m^2 g^{-1}, respectively, for the bulk catalyst to 1092 cm^3 mg^{-1} and 182 m^2 g^{-1}, respectively, for exfoliated g-C_3N_4 [37]. Ultra-thin and porous structures of g-C_3N_4 have been shown to shorten the charge diffusion distance while providing a large surface area for its transfer [23,40]. It is worth noting the disorder that the exfoliation treatment caused in the polymeric structure, as evidenced by increased porosity and surface area, as well as by the strong shifts observed in the absorption and photoluminescence emission spectra [37].

The properties of the g-C_3N_4 suspensions used in the preparation of the supported membranes are presented in Table 1. DLS particle size measurements of bulk g-C_3N_4 suspensions, also shown in Fig. S1a (Supplementary Material, SM), displayed bimodal size distribution with large aggregates in the micron size range, namely with a 745.3 ± 83.3 nm dominant size of aggregates/agglomerates and a secondary peak at 167.8 ± 51.6 nm. Interestingly, the suspensions of the exfoliated material (Table 1, and Fig. S1b) exhibited a well-defined single peak at 257.1 ± 7.8 nm, *i.e.,* about one-third of the dominant size of the bulk material. Therefore, the exfoliation process could be advantageous to obtain improved membranes, since large aggregates/agglomerates and a non-uniform particle size distribution have resulted in cracks when preparing films from suspensions of g-C_3N_4 [41]. Moreover, compared

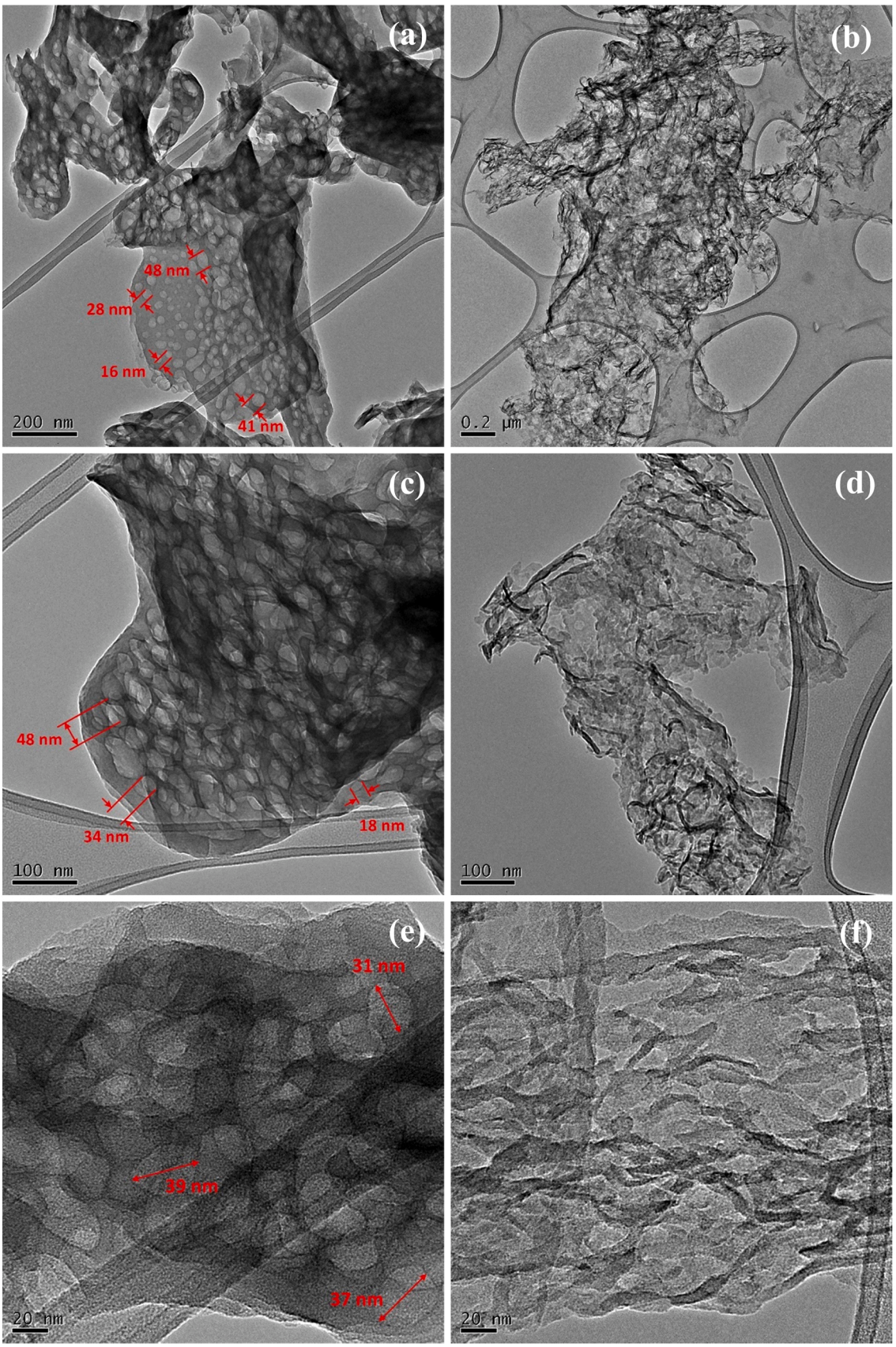

Fig. 2. TEM images of bulk (a, c, e) and exfoliated (b, d, f) g-C_3N_4 in powder form.

Table 1
Properties of bulk and exfoliated g-C_3N_4 suspensions.

	Bulk g-C_3N_4	Exfoliated g-C_3N_4
Concentration (μg mL^{-1})	42	414
DLS particle size (nm)	745.3 ± 83.3 167.8 ± 51.6	257.1 ± 7.8
ζ-Potential (mV)	-34.0 ± 1.1	-22.8 ± 0.6
pH	7.92 ± 0.03	6.91 ± 0.06

to the bulk, stable suspensions with 10 times higher concentration were achieved with exfoliated g-C_3N_4 (Table 1). Bulk and exfoliated g-C_3N_4 were negatively charged at the pH of the suspensions, exhibiting a ζ-potential of −34.0 ± 1.1 mV (pH = 7.92 ± 0.03) and −22.8 ± 0.6 mV (pH = 6.91 ± 0.06), respectively, in agreement with the isoelectric point found in the literature [42,43]. The surface charge of g-C_3N_4 materials depends on the primary, secondary and tertiary amine groups present in their structure, since the first two are considered amphoteric and accept either protons or hydroxyl ions, while the latter can only react with protons [21,43]. As the ζ-potential of PVDF is also negative (*ca.* −40 mV at pH 6.0–8.0), electrostatic repulsions can occur in the polymeric mixture during the fabrication process, which could lead to g-C_3N_4 being placed on the membrane outer surface or on the inner surface of the membrane pores (*i.e.*, always in the surface rather than in bulk), thus favouring the photocatalytic process [24,44].

The crystal structure of the as-synthesised g-C_3N_4 materials in powder form and the respective polymeric composite membranes was characterised by XRD (Fig. 3). Both powder materials exhibited the two characteristic peaks of graphitic carbon nitride, according to the patterrns of the Joint Committee on Powder Diffraction Standards (JCPDS 87–1526). The weak diffraction peak observed at 13.3° was indexed as (100), which is associated with the in-plane structural packing motif of tri-s-triazine units, and the strong diffraction peak at 27.4° corresponds to the (002) plane, attributed to the interlayer stacking of the conjugated aromatic system [19,23,45]. The intensity of the (002) peak was significantly reduced after the exfoliation process, indicating a decrease in the number of aligned layers, more defective structure and a higher degree of amorphization [19,22,40]. The PVDF membrane displayed diffraction peaks at 18.8°, 20.5°, 27.4°, 33.5°, 36.3°, 39.3° and 56.6°, which can be ascribed to the (020), (110), (021), (130), (200), (002) and (300) reflections of its monoclinic α-phase, respectively [46–48]. PVDF membranes prepared with bulk and exfoliated g-C_3N_4, maintained the crystalline characteristics of the powdered materials and the PVDF membrane, as seen in their XRD patterns. The more intense (002) band for both g-C_3N_4-PVDF membranes confirmed the presence of g-C_3N_4, *i.e.*, when compared with the reference PVDF membrane without g-C_3N_4.

The functional groups of the g-C_3N_4 powders and g-C_3N_4-PVDF membranes were identified by FTIR spectroscopy (Fig. 4). Regarding g-C_3N_4 powder materials, the broad band between 3400 and 3000 cm^{-1} was ascribed to O−H and N−H stretching vibrations from physically adsorbed water and partial hydrogenation of N atoms, respectively [49,50]. The multiple bands in the 1650–1200 cm^{-1} region were attributed to the characteristic stretching mode of C−N and C═N [24,30,51]. Specifically, the bands at 1630 and 1560 cm^{-1} were assigned to heterocyclic C═N stretching, while those at 1460, 1400, 1320 and 1235 cm^{-1} were ascribed to C−N stretching vibration of tri-s-triazine [30,51]. The vibration band at 890 cm^{-1} was associated with the N−H deformation mode of amino groups [19,51]. The band at 807 cm^{-1} corresponds to the breathing mode of tri-s-triazine units [52,53]. Exfoliated g-C_3N_4 displayed bands with higher intensity than the bulk material, which may be rationalised by a more ordered packing of tri-s-triazine units [23,54]. The more intense IR bands of stretching aromatic carbon-nitrogen bonds can be related to the simultaneous increase of the 890 cm^{-1} band associated with terminal nitrogen groups (*i.e.*, defects in the matrix). In the FTIR spectra of the polymeric membranes, the corresponding bands of PVDF α-phase were observed, according to the XRD analysis. The vibrational bands at 3025, 2975 and 1065 cm^{-1} were assigned to the C−H stretching vibration [55,56]. The band displayed at 1655 cm^{-1} is characteristic of the C═O stretching of PVP [57]. The vibration bands observed at 1400, 975 and 873 cm^{-1} were attributed to the C−H bending, rocking and wagging vibrations, respectively [58,59]. The bands located at 1881, 800 and 764 cm^{-1} were ascribed to the C−F symmetric stretching, rocking and bending vibrations, respectively [60].

The surface morphology of g-C_3N_4 supported on PTFE and the g-C_3N_4-PVDF polymeric membranes, as well as cross-sectional views of the latter, were investigated by SEM (Fig. 5). SEM images of the reference PVDF membrane are shown in Fig. S2 (SM) for comparison. Top views of the supported membranes (Fig. 5a and b) exhibited a uniformly distributed pattern of layered aggregates in the submicron scale without cracks completely covering the PTFE substrate, and revealed

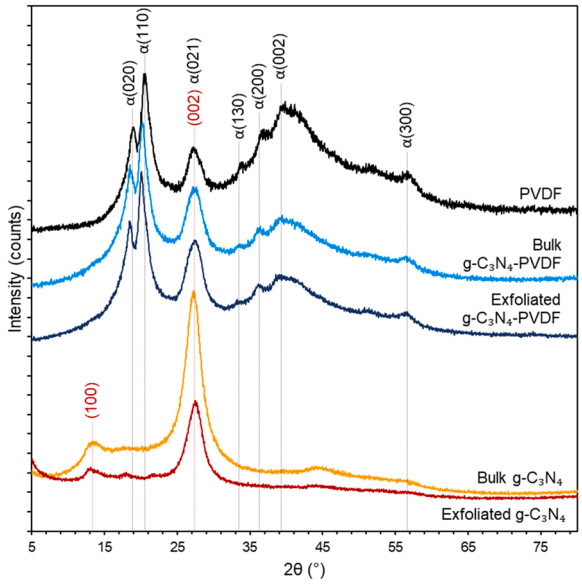

Fig. 3. X-ray diffraction patterns of bulk g-C_3N_4 and exfoliated g-C_3N_4 in powder form, and PVDF, bulk g-C_3N_4-PVDF and exfoliated g-C_3N_4-PVDF membranes.

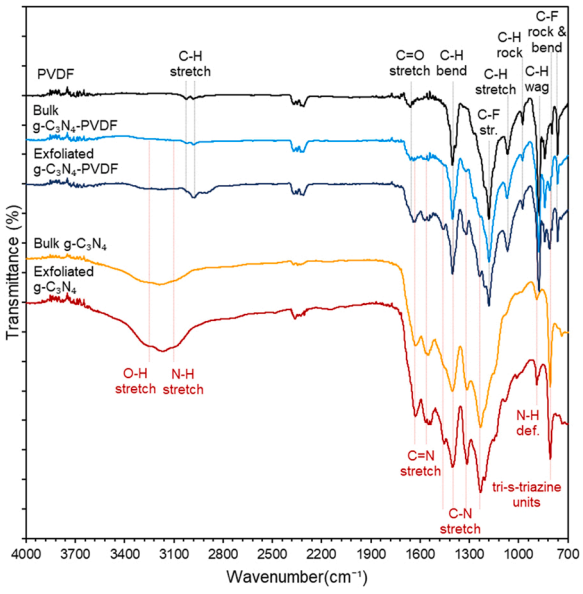

Fig. 4. FTIR-ATR spectra of bulk g-C_3N_4 and exfoliated g-C_3N_4 in powder form, and PVDF, bulk g-C_3N_4-PVDF and exfoliated g-C_3N_4-PVDF membranes.

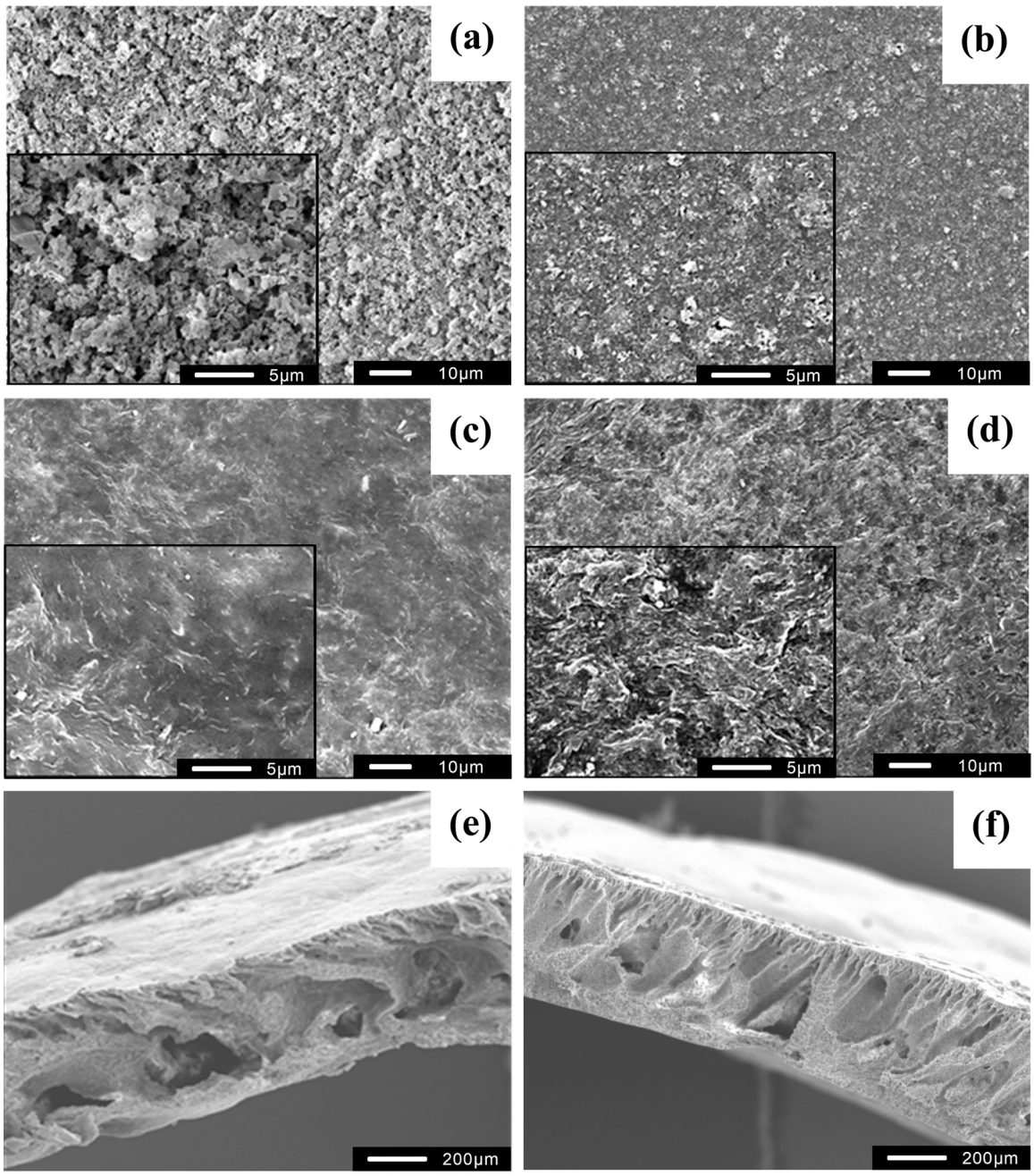

Fig. 5. SEM images of bulk (a) and exfoliated (b) g-C_3N_4 on PTFE membranes; top and cross-sectional SEM images of bulk g-C_3N_4-PVDF (c, e) and exfoliated g-C_3N_4-PVDF (d, f) membranes.

morphological differences when using different g-C_3N_4 powders. g-C_3N_4 supported membranes prepared with the exfoliated material, consisting of remarkably smaller aggregates, displayed a smoother surface than the bulk, in accordance with the DLS results (Table 1 and Fig. S1). Thin catalytic coatings, as those prepared in this work (catalyst surface density of 0.2 mg cm^{-2}), are not only desirable for high water permeability, but it has also been reported that increasing coating thickness did not significantly enhance the photocatalytic activity because the light cannot penetrate from the top layer to the inner layers of the catalyst to activate it [61,62]. For composite membranes to be competitive with supported membranes, a g-C_3N_4 loading of 4.7 wt% was used, as very high loadings of photocatalysts have been shown to form agglomerates, reducing the specific surface area and blocking pores, leading to low photocatalytic degradation efficiency [63]. The reference PVDF membrane and the PVDF polymeric membrane prepared with the bulk g-C_3N_4 material, possessed the same morphological features consisting of a smooth surface and large finger-like channels with macro-voids (Fig. 5c and e; and Fig. S2), suggesting that the bulk photocatalyst was effectively embedded in the polymeric matrix. In contrast, the PVDF composite membrane prepared with exfoliated g-C_3N_4 showed significantly higher surface roughness and the absence of macro-voids (Fig. 5d and f). Both g-C_3N_4-PVDF membranes presented the typical sponge-like asymmetric microstructure of PVDF with a dense top layer, as observed in the cross-sectional SEM images (Fig. 5e and f and Fig. S2b for the reference PVDF membrane). Macro-voids formation has been attributed to the rate increase of solvent (NMP)/non-solvent (distilled water) exchange during the phase inversion process in the presence of a hydrophilic compound (*i.e.*, PVP or the g-C_3N_4 catalyst) that migrates towards the polymer/water interface [64,65]. Although the mass loading of both photocatalysts in the polymeric mixture was the same, the volume of the

exfoliated g-C_3N_4 was notably higher, which could have delayed phase inversion kinetics due to the increase in the viscosity of the casting solution [66]. The membrane thickness could be estimated from cross-sectional SEM images at around 450 μm, barely changing after the addition of g-C_3N_4.

The wettability of the as-fabricated membranes was determined by the sessile drop technique. Regarding g-C_3N_4 materials supported on PTFE membranes, WCA could not be adequately measured as the droplet spread instantly on the surface (WCA $< 20°$), being considered super hydrophilic. PVDF, bulk g-C_3N_4-PVDF and exfoliated g-C_3N_4-PVDF composite membranes were hydrophilic (WCA $< 90°$), yielding WCA values of $64 \pm 6°$, $68 \pm 3°$ and $79 \pm 3°$, respectively (Table S1, SM). Therefore, the surface hydrophilicity was not affected by incorporating the bulk photocatalyst, whereas it became slightly hydrophobic when the exfoliated g-C_3N_4 was added. The amphiphilic character of g-C_3N_4 has been previously described so that the conjugated basal plane and the edge groups constitute the hydrophobic and hydrophilic sections, respectively [67]. The higher WCA values observed for the g-C_3N_4-PVDF membrane prepared with the exfoliated material could also be explained by its higher surface roughness [51].

It is worth noting that the photocatalytic membranes prepared in this work are thermally stable up to the limit imposed by the polymeric material (*i.e.*, PTFE or PVDF), as g-C_3N_4 is thermally stable up to 600 °C due to the aromatic C–N heterocycles [68] and the addition of the catalyst did not lead to changes in crystallinity compared to that of pure PVDF for the composite membrane (Fig. 3). It is known that PTFE membranes are resistant to temperatures up to 500 °C and PVDF membranes are stable at least up to 300–500 °C, barely changing upon the incorporation of a catalyst [69,70]. In terms of mechanical stability, supported membranes suffer from a mechanical detachment of the catalytic film from the substrate [32], therein lies the advantage of embedding the catalyst in the polymer matrix. For instance, it has been reported that the mechanical properties of PVDF membranes can be affected by embedding a nanostructured catalyst into the polymeric matrix, resulting in an increase in tensile strength and a shift from ductile to brittle modes with a concomitant decrease in elongation at the breaking point as the catalyst loading increases, but without comprising its practical application at catalyst loadings below 5 wt% [71–74].

3.2. Photocatalytic filtration performance

The photocatalytic filtration performance of the metal-free g-C_3N_4-based membranes, prepared both by embedding g-C_3N_4 in a PVDF matrix and by vacuum filtration on a PTFE substrate, was evaluated for VFX degradation under constant flow conditions (Fig. 6). Photolytic and dark adsorption experiments were also performed under the same experimental conditions, without membrane (photolysis) and without turning on the LED (dark adsorption). As shown in Fig. S3, photolysis led to a

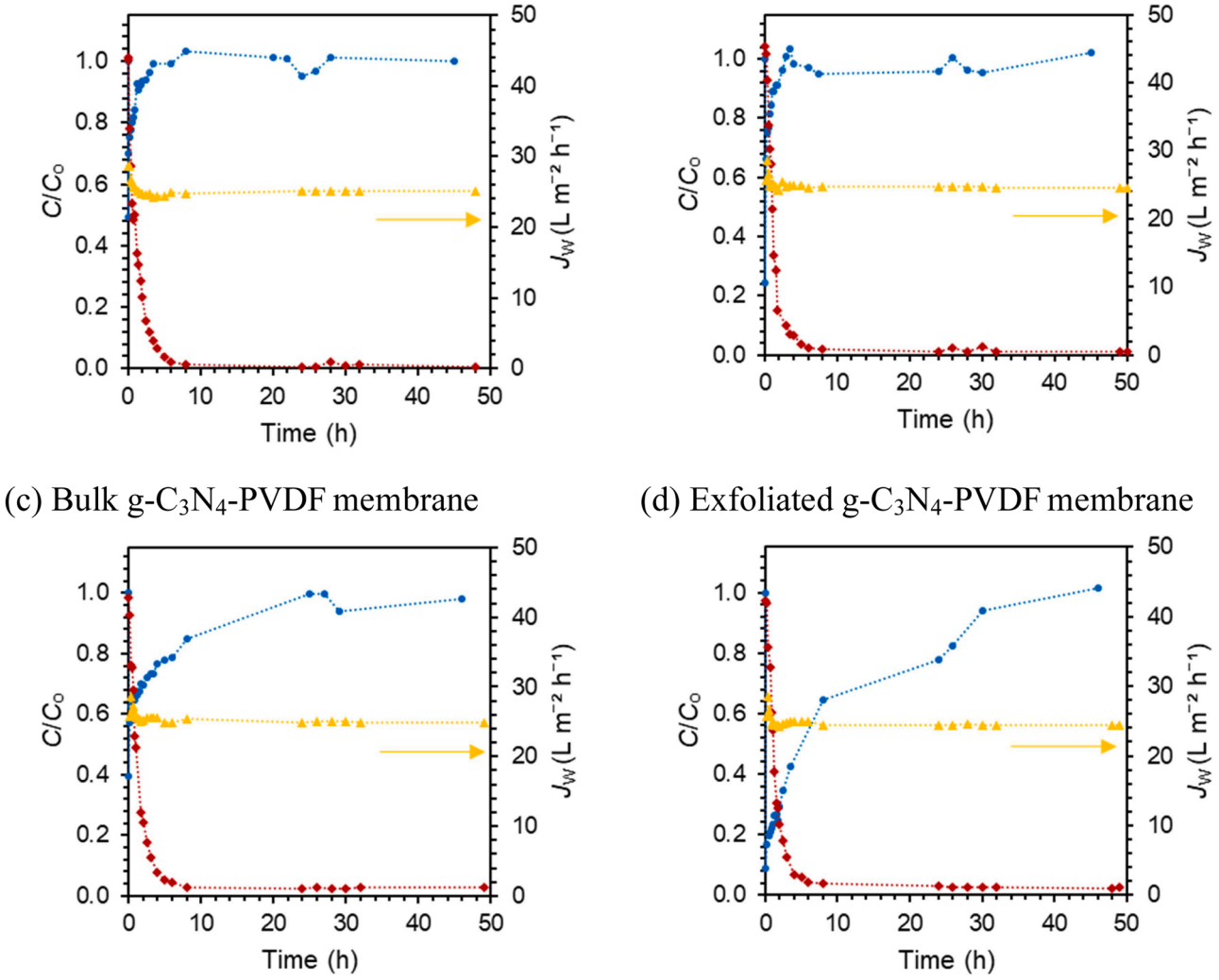

Fig. 6. Normalised VFX concentration obtained in adsorption ● and photocatalytic ◆ experiments performed with ultrapure water, with the bulk (a) and exfoliated (b) g-C_3N_4 supported on PTFE membranes, and bulk (c) and exfoliated (d) g-C_3N_4 mixed in PVDF membranes. Permeate flux (J_W) is also shown for photocatalytic experiments ▲. Experiments performed with $[VFX]_0 = 250$ μg L^{-1}, $pH_0 = 6.2$, $Q = 0.1$ mL min^{-1} (continuous flow mode), and $T = 22 \pm 2$ °C.

decrease of less than 10% in VFX concentration, which remained approximately constant for 6 h. Adsorption experiments with the membranes in dark conditions showed a fast decrease in VFX concentration at the beginning of the process (> 50% removal), which then steadily increased until the removal was negligible as the membranes became saturated. Concerning adsorption capability, notable differences were found between g-C_3N_4 supported on PTFE and g-C_3N_4-PVDF membranes. VFX adsorption was insignificant after 3 h for both g-C_3N_4 (bulk and exfoliated) supported membranes and only after 24 or 46 h of continuous operation, respectively, for bulk and exfoliated g-C_3N_4 mixed in PVDF membranes. The higher adsorption capability of the PVDF membrane prepared with exfoliated g-C_3N_4 is in agreement with its increased surface roughness observed in SEM images, compared to the PVDF membrane with bulk g-C_3N_4 (Fig. 5). After the adsorption process, the light was switched on, and the photocatalytic filtration reaction started, achieving a VFX removal above 95% after the first 5 h of visible irradiation for all tested membranes. Furthermore, the VFX concentration in the effluent was kept negligible for up to 48 h of continuous operation, corresponding to a VFX mass removal rate of about 6 mg m^{-2} h^{-1} (Eq. 2). A pseudo-first order kinetic model was fitted to the experimental data for the photocatalytic degradation of VFX (Fig. S4, SM). The kinetic constants (k) were respectively found to be 0.0118 and 0.0122 min^{-1} for bulk and exfoliated g-C_3N_4 supported on PTFE membranes, and 0.0113 and 0.0115 min^{-1} for bulk and exfoliated g-C_3N_4 mixed in PVDF membranes. As the results indicate, the as-fabricated g-C_3N_4-based membranes did not exhibit significant differences in the photocatalytic filtration performance for VFX degradation despite their different morphological characteristics and adsorption capabilities. Moreover, the permeate flux (J_W) remained constant after the first 30 min of photocatalytic reactions in continuous flow mode with a value of approximately 25 L m^{-2} h^{-1} for all tested membranes (Eq. 1), as also shown in Fig. 6. Thereby, fouling (or possible deactivation) was negligible in these experiments, and the higher hydrophobicity of the polymeric membranes compared to those supported did not affect the permeate flux. Membrane scale-up depends mainly on the maximum volumetric throughput or capacity, which is limited by filter fouling [75]. Fouling causes the permeate flux to decrease, restricting the volume of water that can be filtered with a given membrane area. In this work, membranes with an effective area of 2.1 cm^2 were used, which is in the same range as those employed in other photocatalytic filtration studies for water treatment (Table S2). Effective membrane area must be increased when the filtration requirements of the process are not met due to membrane fouling. Therefore, the design of a dead-end filtration system involves estimating the membrane area required for a given fluid volume and specified operating conditions [76].

The photocatalytic mechanism of metal-free g-C_3N_4-based materials for the degradation of aromatic molecules is mainly attributed to the generation of reactive oxygen species (ROS), along with the photo-induced holes [77]. Upon irradiation at the appropriate wavelength, electrons in the valence band (VB) are promoted to the conduction band (CB) of g-C_3N_4 creating electron-hole pairs (g-$C_3N_4 + h\nu \rightarrow e^- + h^+$) that will be readily available to induce redox reactions. When dissolved oxygen is present, it can be reduced by the photoexcited electrons through a one-electron reduction route to superoxide radicals ($O_2 + e^- \rightarrow O_2^{\bullet-}$) [78]. Additionally, H_2O_2 can be produced by a two-electron reduction pathway from oxygen ($O_2 + 2e^- + 2\,H^+ \rightarrow H_2O_2$) and subsequently reduced to $HO^\bullet$ ($H_2O_2 + e^- \rightarrow HO^- + HO^\bullet$) [14,21,77,79]. $O_2^{\bullet-}$ and $HO^\bullet$ have a strong oxidative capacity and participate in reactions involving other oxidants, globally referred to as ROS. It has been demonstrated that the thermal exfoliation treatment provides g-C_3N_4 with increased surface area, leading to higher availability of actives sites and, thus, faster degradation rates and H_2O_2 yields [21,23,80–82]. However, the influence of this parameter on the photocatalytic performance is minimised when the photocatalyst is immobilised, either supported or embedded, which could explain the similar results obtained for bulk and exfoliated g-C_3N_4 photocatalysts in this work. Unexpectedly, the photocatalytic filtration performance of g-C_3N_4-PVDF membranes practically equalled that of the supported ones. It is known that a large amount of photocatalyst is buried within the polymeric matrix when membranes are prepared by embedding/phase inversion, which drastically diminishes the number of active sites [32,34]. Nevertheless, the negative ζ-potential of g-C_3N_4 and PVDF could have overcome this limitation by locating the photocatalyst on the membrane's outer surface or the inner surface of the pores during the fabrication process, as stated previously. The low compatibility of the g-C_3N_4-based materials with the polymer matrix has often led to catalyst aggregation, reducing membrane separation properties, which has been counteracted by g-C_3N_4 functionalisation or interface agent addition [83].

In this work, g-C_3N_4 showed good dispersibility in the polymeric matrix (PVDF) most probably due to its small particle size (Table 1), large surface area (Fig. 2) and high availability of N−H end groups (Fig. 4). Furthermore, the fabrication of g-C_3N_4-PVDF polymeric membranes is scalable and highly reproducible compared to the supported membranes prepared by vacuum filtration, which also need a substrate and present some challenges regarding their reusability due to the relatively poor adhesion of the photocatalyst to the support [32,34]. As the energy costs of the exfoliation process do not compensate in this case, and since these polymeric membranes are more promising for industrial applications than the supported ones, PVDF membranes prepared with bulk g-C_3N_4 were selected for further VFX degradation studies using scavengers and surface water (SW) as a matrix.

The main active species during the photocatalytic degradation of VFX using PVDF membranes prepared with bulk g-C_3N_4 were investigated by short (2.5 h) quenching experiments. As shown in Fig. S5 (SM), the addition of *p*-BQ had little effect on VFX degradation (< 10% at 150 min) compared to the control (no scavenger), suggesting the minor contribution of $O_2^{\bullet-}$ radicals. In contrast, the addition of MeOH and NaN_3 inhibited VFX degradation to some extent (approximately 30%), while dosing with EDTA produced an even higher inhibition (> 50%) at 150 min of reaction. These results suggest that the photogenerated h^+ played an important role during the photocatalytic process. In previous studies, it was found that $O_2^{\bullet-}$ and h^+ were the main reactive species responsible for the removal of contaminants [84,85]. For instance, a g-C_3N_4 catalyst, prepared by thermal decomposition of dicyandiamide at 550 °C and subsequent thermal exfoliation at 500 °C, was tested for the photocatalytic degradation of two micropollutants, metoprolol (MET) and diclofenac (DCF), under visible-light illumination [84]. Experiments using EDTA and *tert*-butanol (*t*-BuOH) as scavengers revealed that the degradation of both micropollutants (individually or as a mixture) was mainly affected by h^+ and $HO^\bullet$. Conversely, quenching studies indicated that the photocatalytic degradation of ethyl-parabens (EP) was significantly inhibited by *p*-BQ and triethanolamine (TEOA), suggesting that $O_2^{\bullet-}$ radicals and photoinduced h^+ played a crucial role, while barely affected by *t*-BuOH [85]. In the present study, the mechanism seems different, as $O_2^{\bullet-}$ radicals hardly contributed to VFX degradation, which can be explained as follows. First, as described above, the $O_2^{\bullet-}$ generated by g-C_3N_4 upon light activation may be reduced by photoexcited e^- to H_2O_2, which can be further reduced leading to $HO^\bullet$. In addition, the reaction between $O_2^{\bullet-}$ and h^+ generates $^1O_2$ according to previous reports [86,87], which has been shown to contribute to VFX degradation. Thus, more research is needed in this domain to better understand the reaction mechanism.

The photocatalytic removal of VFX (after the adsorption process) in SW using a g-C_3N_4-PVDF polymeric membrane is shown in Fig. 7, and the results were compared to the performance of the same membrane under the same experimental conditions but using ultrapure water. Pseudo-first order kinetics are also displayed in Fig. S4 (SM). As can be observed, the efficiency of the photocatalytic filtration process dramatically decreased when using SW (k = 0.0028 min^{-1}); however, a relatively high VFX removal of 50% (corresponding to 3 mg m^{-2} h^{-1}, Eq. 2) was achieved at a steady state. Interestingly, the permeate flux (J_W) was also around 25 L m^{-2} h^{-1} in this case and did not decrease

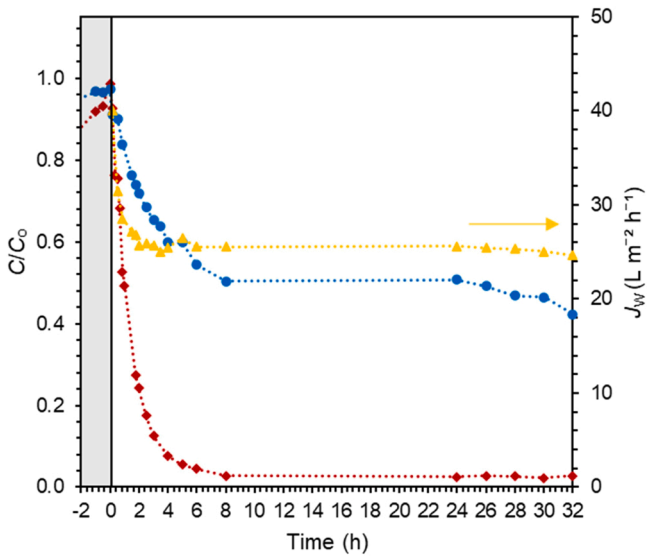

Fig. 7. Normalised concentration of VFX in photocatalysis with PVDF membranes prepared with bulk g-C_3N_4 in surface water (SW, ●). Experiments performed with $[VFX]_0 = 250\ \mu g\ L^{-1}$, $pH_0 = 7.5$, $Q = 0.1\ mL\ min^{-1}$ (continuous flow mode), and $T = 22 \pm 2\ °C$. Permeate flux (J_W, ▲) and the results of the photocatalytic experiment performed in ultrapure water (◆) are also shown.

throughout the experiment, indicating that fouling did not occur or not affect the filtration capability after 32 h of continuous operation with SW.

The physicochemical properties of natural water, as well as its content of organic and inorganic species, have been shown to negatively affect the efficiency of photocatalytic filtration processes [32,88]. Natural organic matter and the target pollutant could compete in the adsorption process, while some inorganic ions (*i.e.*, Cl^-, NO_3^-, Na^+, K^+, Ca^{2+}, Mg^{2+}, NH_4^+ or SO_4^{2-}) [89] that are widely present in SW could scavenge photogenerated ROS [90–92]. The present study has been carried out under realistic conditions, not only with real water matrices (SW), but also with a low micropollutant concentration ($250\ \mu g\ L^{-1}$ VFX) and a long reaction time (48 or 32 h), when compared with most of the previously conducted studies. Effective membrane area and initial micropollutant concentration are parameters that could be also studied, together with visible-light intensity and flow rate (or retention time) for a given water matrix. However, VFX concentrations much higher than the one used here are rarely found in the environment [8], and lower concentrations would make accurate quantification more difficult. Our findings are in line with the limitations mentioned above, highlighting the need for research efforts for real water or wastewater treatment (instead of simulated water or wastewater) to better understand the synergy between membrane filtration and photocatalysis and promote their practical applications.

4. Conclusions

Carbon nitride-based membranes were shown to be effective for venlafaxine degradation by simultaneous photocatalytic and membrane filtration processes under visible-light irradiation and in continuous flow mode operation. Membranes fabricated by embedding g-C_3N_4 in PVDF, matched the same results obtained for those supported on a PTFE substrate, despite their different configurations. The porous nature of the synthesised g-C_3N_4, and the small particle size and available terminal functional groups, are beneficial to obtain good dispersibility in the prepared membranes. However, it was demonstrated that the exfoliation process of g-C_3N_4 has little influence when the catalyst is immobilised.

Venlafaxine removals above 95% were achieved after 5 h of visible-light irradiation (418 nm with an irradiance of $11.2\ W\ m^{-2}$) for all prepared membranes. These high removals were maintained for up to 48 h of continuous operation. When surface water was used instead of ultrapure water, conversions of 50% were reached despite the complexity of the real matrix and the presence of competing ions that can scavenge the reactive species generated during the photocatalytic process. Furthermore, the permeate flux was determined throughout the experiments, proving that even after long periods of operation fouling was not detected at these conditions for these membranes.

CRediT authorship contribution statement

Laura Valenzuela: Investigation, Conceptualization, Formal analysis, Methodology, Writing – original draft. **Marta Pedrosa:** Investigation, Conceptualization, Formal analysis, Methodology, Writing – original draft. **Ana Bahamonde:** Writing – review & editing, Supervision, Resources. **Roberto Rosal:** Writing – review & editing, Supervision, Resources. **André Torres-Pinto**: Investigation, Conceptualization, Writing – review & editing. **Cláudia G. Silva**: Conceptualization, Resources, Writing – review & editing. **Joaquim L. Faria**: Conceptualization, Resources, Writing – review & editing. **Adrián M.T. Silva**: Conceptualization, Resources, Project administration, Funding acquisition, Writing – review & editing, Supervision.

Declaration of Competing Interest

The authors declare that they have no known competing financial interests or personal relationships that could have appeared to influence the work reported in this paper.

Data Availability

Data will be made available on request.

Acknowledgements

LV thanks the Spanish Ministry of Education for the FPU grant FPU17/03096 and the Spanish Ministry of Universities for the visiting research fellowship EST19/00759. A.T-P. acknowledges *Fundação para a Ciência e a Tecnologia* (FCT) for his scholarship SFRH/BD/143487/2019. This work was financially supported by the project Healthy Waters - Identification, Elimination, Social Awareness and Education of Water Chemical and Biological Micropollutants with Health and Environmental Implications, with reference NORTE-01–0145-FEDER-000069, and ClimActiC - Connecting Citizenship and Science for Climate Adaptation, with reference NORTE-01–0145-FEDER-000071, supported by Norte Portugal Regional Operational Programme (NORTE 2020), under the PORTUGAL 2020 Partnership Agreement through the European Regional Development Fund (ERDF). We would also like to thank the scientific collaboration under LA/P/0045/2020 (ALiCE), UIDB/50020/2020 and UIDP/50020/2020 (LSRE-LCM), funded by national funds through FCT/MCTES (PIDDAC).

Appendix A. Supporting information

Supplementary data associated with this article can be found in the online version at doi:10.1016/j.cattod.2023.114042.

References

[1] M.O. Barbosa, N.F.F. Moreira, A.R. Ribeiro, M.F.R. Pereira, A.M.T. Silva, Occurrence and removal of organic micropollutants: an overview of the watch list of EU decision 2015/495, Water Res. 94 (2016) 257–279.
[2] M.R. Pino-Otín, S. Muñiz, J. Val, E. Navarro, Effects of 18 pharmaceuticals on the physiological diversity of edaphic microorganisms, Sci. Total Environ. 595 (2017) 441–450.

[3] M. Zhang, Y. Yang, X. An, L.-a Hou, A critical review of g-C3N4-based photocatalytic membrane for water purification, Chem. Eng. J. 412 (2021), 128663.

[4] N. Diaz-Camal, J.D. Cardoso-Vera, H. Islas-Flores, L.M. Gómez-Oliván, A. Mejía-García, Consumption and ocurrence of antidepressants (SSRIs) in pre- and post-COVID-19 pandemic, their environmental impact and innovative removal methods: a review, Sci. Total Environ. 829 (2022), 154656.

[5] D. Lambropoulou, E. Evgenidou, V. Saliverou, C. Kosma, I. Konstantinou, Degradation of venlafaxine using TiO2/UV process: Kinetic studies, RSM optimization, identification of transformation products and toxicity evaluation, J. Hazard. Mater. 323 (2017) 513–526.

[6] R.A. Osawa, B.T. Barrocas, O.C. Monteiro, M. Conceição Oliveira, M.H. Florêncio, Photocatalytic degradation of amitriptyline, trazodone and venlafaxine using modified cobalt-titanate nanowires under UV–Vis radiation: transformation products and in silico toxicity, Chem. Eng. J. 373 (2019) 1338–1347.

[7] M. Papageorgiou, C. Kosma, D. Lambropoulou, Seasonal occurrence, removal, mass loading and environmental risk assessment of 55 pharmaceuticals and personal care products in a municipal wastewater treatment plant in Central Greece, Sci. Total Environ. 543 (2016) 547–569.

[8] H. Rapp-Wright, F. Regan, B. White, L.P. Barron, A year-long study of the occurrence and risk of over 140 contaminants of emerging concern in wastewater influent, effluent and receiving waters in the Republic of Ireland, Sci. Total Environ. 860 (2023), 160379.

[9] P.C. Rúa-Gómez, W. Püttmann, Degradation of lidocaine, tramadol, venlafaxine and the metabolites O-desmethyltramadol and O-desmethylvenlafaxine in surface waters, Chemosphere 90 (2013) 1952–1959.

[10] N.F.F. Moreira, C. Narciso-da-Rocha, M.I. Polo-López, L.M. Pastrana-Martínez, J. L. Faria, C.M. Manaia, P. Fernández-Ibáñez, O.C. Nunes, A.M.T. Silva, Solar treatment (H2O2, TiO2-P25 and GO-TiO2 photocatalysis, photo-Fenton) of organic micropollutants, human pathogen indicators, antibiotic resistant bacteria and related genes in urban wastewater, Water Res. 135 (2018) 195–206.

[11] N.F.F. Moreira, M.J. Sampaio, A.R. Ribeiro, C.G. Silva, J.L. Faria, A.M.T. Silva, Metal-free g-C3N4 photocatalysis of organic micropollutants in urban wastewater under visible light, Appl. Catal. B: Environ. 248 (2019) 184–192.

[12] X. Duan, H. Sun, S. Wang, Metal-free carbocatalysis in advanced oxidation reactions, Acc. Chem. Res. 51 (2018) 678–687.

[13] W.-K. Jo, S. Kumar, S. Eslava, S. Tonda, Construction of Bi2WO6/RGO/g-C3N4 2D/2D/2D hybrid Z-scheme heterojunctions with large interfacial contact area for efficient charge separation and high-performance photoreduction of CO2 and H2O into solar fuels, Appl. Catal. B: Environ. 239 (2018) 586–598.

[14] L. Jiang, X. Yuan, G. Zeng, Z. Wu, J. Liang, X. Chen, L. Leng, H. Wang, H. Wang, Metal-free efficient photocatalyst for stable visible-light photocatalytic degradation of refractory pollutant, Appl. Catal. B: Environ. 221 (2018) 715–725.

[15] J. Wen, J. Xie, X. Chen, X. Li, A review on g-C3N4-based photocatalysts, Appl. Surf. Sci. 391 (2017) 72–123.

[16] I. Velo-Gala, A. Torres-Pinto, C.G. Silva, B. Ohtani, A.M.T. Silva, J.L. Faria, Graphitic carbon nitride photocatalysis: the hydroperoxyl radical role revealed by kinetic modelling, Catal. Sci. Technol. 11 (2021) 7712–7726.

[17] C. Casado, R. Timmers, A. Sergejevs, C.T. Clarke, D.W.E. Allsopp, C.R. Bowen, R. van Grieken, J. Marugán, Design and validation of a LED-based high intensity photocatalytic reactor for quantifying activity measurements, Chem. Eng. J. 327 (2017) 1043–1055.

[18] G. Matafonova, V. Batoev, Recent advances in application of UV light-emitting diodes for degrading organic pollutants in water through advanced oxidation processes: a review, Water Res. 132 (2018) 177–189.

[19] I. Papailias, N. Todorova, T. Giannakopoulou, N. Ioannidis, N. Boukos, C. P. Athanasekou, D. Dimotikali, C. Trapalis, Chemical vs thermal exfoliation of g-C3N4 for NOx removal under visible light irradiation, Appl. Catal. B: Environ. 239 (2018) 16–26.

[20] W.-J. Ong, L.-L. Tan, Y.H. Ng, S.-T. Yong, S.-P. Chai, Graphitic carbon nitride (g-C3N4)-based photocatalysts for artificial photosynthesis and environmental remediation: are we a step closer to achieving sustainability? Chem. Rev. 116 (2016) 7159–7329.

[21] A. Torres-Pinto, M.J. Sampaio, C.G. Silva, J.L. Faria, A.M.T. Silva, Metal-free carbon nitride photocatalysis with in situ hydrogen peroxide generation for the degradation of aromatic compounds, Appl. Catal. B: Environ. 252 (2019) 128–137.

[22] Y.-J. Yuan, Z. Shen, S. Wu, Y. Su, L. Pei, Z. Ji, M. Ding, W. Bai, Y. Chen, Z.-T. Yu, Z. Zou, Liquid exfoliation of g-C3N4 nanosheets to construct 2D–2D MoS2/g-C3N4 photocatalyst for enhanced photocatalytic H2 production activity, Appl. Catal. B: Environ. 246 (2019) 120–128.

[23] M. Zhang, Y. Yang, X. An, J. Zhao, Y. Bao, L.-a Hou, Exfoliation method matters: the microstructure-dependent photoactivity of g-C3N4 nanosheets for water purification, J. Hazard. Mater. 424 (2022), 127424.

[24] Y. Cui, L. Yang, J. Zheng, Z. Wang, B. Li, Y. Yan, M. Meng, Synergistic interaction of Z-scheme 2D/3D g-C3N4/BiOI heterojunction and porous PVDF membrane for greatly improving the photodegradation efficiency of tetracycline, J. Colloid Interface Sci. 586 (2021) 335–348.

[25] C. Hu, M.-S. Wang, C.-H. Chen, Y.-R. Chen, P.-H. Huang, K.-L. Tung, Phosphorus-doped g-C3N4 integrated photocatalytic membrane reactor for wastewater treatment, J. Membr. Sci. 580 (2019) 1–11.

[26] Y. Liu, Z. Yu, X. Li, L. Shao, H. Zeng, Super hydrophilic composite membrane with photocatalytic degradation and self-cleaning ability based on LDH and g-C3N4, J. Membr. Sci. 617 (2021), 118504.

[27] S. Salehian, H. Heydari, M. Khansanami, V. Vatanpour, S.A. Mousavi, Fabrication and performance of polysulfone/H2O2-g-C3N4 mixed matrix membrane in a photocatalytic membrane reactor under visible light irradiation for removal of natural organic matter, Sep. Purif. Technol. 285 (2022), 120291.

[28] Y. Song, Y. Li, X. Chen, C. Meng, S. Ma, T. Li, K. Jiang, C. Hu, Simultaneous degradation and separation of antibiotics in sewage effluent by photocatalytic nanofiltration membrane in a continuous dynamic process, Water Res. 229 (2023), 119460.

[29] H.B. Truong, B.T. Huy, S.K. Ray, Y.-I. Lee, J. Cho, J. Hur, H2O2-assisted photocatalysis for removal of natural organic matter using nanosheet C3N4-WO3 composite under visible light and the hybrid system with ultrafiltration, Chem. Eng. J. 399 (2020), 125733.

[30] J. Wan, J. Huang, H. Yu, L. Liu, Y. Shi, C. Liu, Fabrication of self-assembled 0D–2D Bi2MoO6-g-C3N4 photocatalytic composite membrane based on PDA intermediate coating with visible light self-cleaning performance, J. Colloid Interface Sci. 601 (2021) 229–241.

[31] S. Mozia, P. Argurio, R. Molinari, Chapter 4 - PMRs utilizing pressure-driven membrane techniques, in: A. Basile, S. Mozia, R. Molinari (Eds.), Current Trends and Future Developments on (Bio-) Membranes, Elsevier, 2018, pp. 97–127.

[32] X. Li, G. Huang, X. Chen, J. Huang, M. Li, J. Yin, Y. Liang, Y. Yao, Y. Li, A review on graphitic carbon nitride (g-C3N4) based hybrid membranes for water and wastewater treatment, in: Sci. Total Environ, 792, 2021, 148462.

[33] J. Song, X. Wu, M. Zhang, C. Liu, J. Yu, G. Sun, Y. Si, B. Ding, Highly flexible, core-shell heterostructured, and visible-light-driven titania-based nanofibrous membranes for antibiotic removal and E. coil inactivation, Chem. Eng. J. 379 (2020), 122269.

[34] Y. Wang, B. Gao, Q. Yue, Z. Wang, Graphitic carbon nitride (g-C3N4)-based membranes for advanced separation, J. Mater. Chem. A 8 (2020) 19133–19155.

[35] S.S. Chin, K. Chiang, A.G. Fane, The stability of polymeric membranes in a TiO2 photocatalysis process, J. Membr. Sci. 275 (2006) 202–211.

[36] Decision (EU), of 22 July 2022 establishing a watch list of substances for Union-wide monitoring in the field of water policy pursuant to directive 2008/105/EC of the European Parliament and of the council off, J. Eur. Union (2022/1307) 2022.

[37] A. Torres-Pinto, C.G. Silva, J.L. Faria, A.M.T. Silva, The effect of precursor selection on the microwave-assisted synthesis of graphitic carbon nitride, Catal. Today (2022).

[38] O. Vieira, R.S. Ribeiro, M. Pedrosa, A.R. Lado Ribeiro, A.M.T. Silva, Nitrogen-doped reduced graphene oxide – PVDF nanocomposite membrane for persulfate activation and degradation of water organic micropollutants, Chem. Eng. J. 402 (2020), 126117.

[39] Y. Yuan, T.R. Lee, Contact angle and wetting properties, in: G. Bracco, B. Holst (Eds.), Surface Science Techniques, Springer Berlin Heidelberg, Berlin, Heidelberg, 2013, pp. 3–34.

[40] H. Zhao, S. Chen, X. Quan, H. Yu, H. Zhao, Integration of microfiltration and visible-light-driven photocatalysis on g-C3N4 nanosheet/reduced graphene oxide membrane for enhanced water treatment, in: Appl. Catal. B: Environ, 194, 2016, pp. 134–140.

[41] L. Wang, Y. Tong, J. Feng, J. Hou, J. Li, X. Hou, J. Liang, G-C3N4-based films: a rising star for photoelectrochemical water splitting, Sustain. Mater. Technol. 19 (2019), e00089.

[42] P. Xia, B. Zhu, J. Yu, S. Cao, M. Jaroniec, Ultra-thin nanosheet assemblies of graphitic carbon nitride for enhanced photocatalytic CO_2 reduction, J. Mater. Chem. A 5 (2017) 3230–3238.

[43] B. Zhu, P. Xia, W. Ho, J. Yu, Isoelectric point and adsorption activity of porous g-C3N4, Appl. Surf. Sci. 344 (2015) 188–195.

[44] Q. Ding, H. Yamamura, N. Murata, N. Aoki, H. Yonekawa, A. Hafuka, Y. Watanabe, Characteristics of meso-particles formed in coagulation process causing irreversible membrane fouling in the coagulation-microfiltration water treatment, Water Res. 101 (2016) 127–136.

[45] W. Ho, Z. Zhang, M. Xu, X. Zhang, X. Wang, Y. Huang, Enhanced visible-light-driven photocatalytic removal of NO: Effect on layer distortion on g-C3N4 by H2 heating, Appl. Catal. B: Environ. 179 (2015) 106–112.

[46] X. Cai, T. Lei, D. Sun, L. Lin, A critical analysis of the α, β and γ phases in poly (vinylidene fluoride) using FTIR, RSC Adv. 7 (2017) 15382–15389.

[47] K. Jurczuk, A. Galeski, M. Mackey, A. Hiltner, E. Baer, Orientation of PVDF α and γ crystals in nanolayered films, Colloid Polym. Sci. 293 (2015) 1289–1297.

[48] K. Shi, B. Sun, X. Huang, P. Jiang, Synergistic effect of graphene nanosheet and BaTiO3 nanoparticles on performance enhancement of electrospun PVDF nanofiber mat for flexible piezoelectric nanogenerators, Nano Energy 52 (2018) 153–162.

[49] P. Qiu, H. Chen, C. Xu, N. Zhou, F. Jiang, X. Wang, Y. Fu, Fabrication of an exfoliated graphitic carbon nitride as a highly active visible light photocatalyst, J. Mater. Chem. A 3 (2015) 24237–24244.

[50] H. Zhao, H. Yu, X. Quan, S. Chen, Y. Zhang, H. Zhao, H. Wang, Fabrication of atomic single layer graphitic-C3N4 and its high performance of photocatalytic disinfection under visible light irradiation, Appl. Catal. B: Environ. 152-153 (2014) 46–50.

[51] S. Seyyed Shahabi, N. Azizi, V. Vatanpour, Synthesis and characterization of novel g-C3N4 modified thin film nanocomposite reverse osmosis membranes to enhance desalination performance and fouling resistance, Sep. Purif. Technol. 215 (2019) 430–440.

[52] I. Ciria-Ramos, N. Navascués, F. Diaw, C. Furgeaud, R. Arenal, A. Ansón-Casaos, M. Haro, E.J. Juarez-Perez, Formamidinium halide salts as precursors of carbon nitrides, Carbon 196 (2022) 1035–1046.

[53] Y.-P. Yuan, L.-S. Yin, S.-W. Cao, L.-N. Gu, G.-S. Xu, P. Du, H. Chai, Y.-S. Liao, C. Xue, Microwave-assisted heating synthesis: a general and rapid strategy for large-scale production of highly crystalline g-C3N4 with enhanced photocatalytic H2 production, Green. Chem. 16 (2014) 4663–4668.

[54] F. Dong, Y. Li, Z. Wang, W.-K. Ho, Enhanced visible light photocatalytic activity and oxidation ability of porous graphene-like g-C3N4 nanosheets via thermal exfoliation, Appl. Surf. Sci. 358 (2015) 393–403.
[55] H. Dong, K. Xiao, X. Tang, Z. Zhang, J. Dai, R. Long, W. Liao, Preparation and characterization of polyurethane (PU)/polyvinylidene fluoride (PVDF) blending membrane, Desalin. Water Treat. 57 (2016) 3405–3413.
[56] Y. Guo, C. Liu, W. Xu, G. Liu, K. Xiao, H.-Z. Zhao, Interpenetrating network nanoarchitectonics of antifouling poly(vinylidene fluoride) membranes for oil–water separation, RSC Adv. 11 (2021) 31865–31876.
[57] C. Yu, W. He, Y. Yan, J. Song, W. Xing, M. Meng, J. Gao, Y. Yan, Y. Wu, Z. Ma, A deep insight for TBBPA imprinting on PVP-assisted separation membrane: Elucidation of detailed chemical transition in membrane preparation and imprinting process, Chem. Eng. J. 436 (2022), 135024.
[58] N. Daems, S. Milis, R. Verbeke, A. Szymczyk, P.P. Pescarmona, I.F.J. Vankelecom, High-performance membranes with full pH-stability, RSC Adv. 8 (2018) 8813–8827.
[59] Y. Fu, Y. Cheng, C. Chen, D. Li, W. Zhang, Study on preparation process and enhanced piezoelectric performance of pine-needle-like ZnO@PVDF composite nanofibers, Polym. Test. 108 (2022), 107513.
[60] Y. Bormashenko, R. Pogreb, O. Stanevsky, E. Bormashenko, Vibrational spectrum of PVDF and its interpretation, Polym. Test. 23 (2004) 791–796.
[61] H. Choi, E. Stathatos, D.D. Dionysiou, Sol–gel preparation of mesoporous photocatalytic TiO2 films and TiO2/Al2O3 composite membranes for environmental applications, Appl. Catal. B: Environ. 63 (2006) 60–67.
[62] L.L. Coelho, M. Grao, T. Pomone, M. Ratova, P. Kelly, M. Wilhelm, R.F.M. Moreira, Photocatalytic microfiltration membranes produced by magnetron sputtering with self-cleaning capabilities, Thin Solid Films 747 (2022), 139143.
[63] S. Kundu, N. Karak, Polymeric photocatalytic membrane: an emerging solution for environmental remediation, Chem. Eng. J. 438 (2022), 135575.
[64] B. Khan, S. Haider, R. Khurram, Z. Wang, X. Wang, Preparation of an ultrafiltration (UF) membrane with narrow and uniform pore size distribution via etching of SiO2 nano-particles in a membrane matrix, Membranes 10 (2020).
[65] M. Meng, B. Li, Y. Zhu, Y. Yan, Y. Feng, A novel mixed matrix polysulfone membrane for enhanced ultrafiltration and photocatalytic self-cleaning performance, J. Colloid Interface Sci. 599 (2021) 178–189.
[66] T. Arumugham, R.G. Amimodu, N.J. Kaleekkal, D. Rana, Nano CuO/g-C3N4 sheets-based ultrafiltration membrane with enhanced interfacial affinity, antifouling and protein separation performances for water treatment application, J. Environ. Sci. 82 (2019) 57–69.
[67] J. Xu, M. Antonietti, The performance of nanoparticulate graphitic carbon nitride as an amphiphile, J. Am. Chem. Soc. 139 (2017) 6026–6029.
[68] X. Wang, S. Blechert, M. Antonietti, Polymeric graphitic carbon nitride for heterogeneous photocatalysis, ACS Catal. 2 (2012) 1596–1606.
[69] C. Liao, J. Zhao, P. Yu, H. Tong, Y. Luo, Synthesis and characterization of SBA-15/poly (vinylidene fluoride) (PVDF) hybrid membrane, Desalination 260 (2010) 147–152.
[70] J.-Y. Park, J.-H. Lee, C.-H. Kim, Y.-J. Kim, Fabrication of polytetrafluoroethylene nanofibrous membranes for guided bone regeneration, RSC Adv. 8 (2018) 34359–34369.
[71] H. Nawaz, M. Umar, I. Nawaz, Q. Zia, M. Tabassum, H. Razzaq, H. Gong, X. Zhao, X. Liu, Photodegradation of textile pollutants by nanocomposite membranes of polyvinylidene fluoride integrated with polyaniline–titanium dioxide nanotubes, Chem. Eng. J. 419 (2021), 129542.
[72] H. Rawindran, J.-W. Lim, P.-S. Goh, M.N. Subramaniam, A.F. Ismail, N.M. Radi bin Nik, M. Daud, M. Rezaei-Dasht, Arzhandi, Simultaneous separation and degradation of surfactants laden in produced water using PVDF/TiO2 photocatalytic membrane, J. Clean. Prod. 221 (2019) 490–501.
[73] G. Yi, J. Li, L.C. Henderson, W. Lei, L. Du, S. Zhao, Enhancing thermal conductivity of polyvinylidene fluoride composites by carbon fiber: length effect of the filler, Polym. (Basel) (2022).
[74] J. Zhao, C. Liao, J. Liu, X. Shen, H. Tong, Development of mesoporous titanium dioxide hybrid poly(vinylidene fluoride) ultrafiltration membranes with photocatalytic properties, J. Appl. Polym. Sci. 133 (2016).
[75] M.E. Laska, R.P. Brooks, M. Gayton, N.S. Pujar, Robust scale-up of dead end filtration: impact of filter fouling mechanisms and flow distribution, Biotechnol. Bioeng. 92 (2005) 308–320.
[76] S. Haindl, J. Stark, J. Dippel, S. Handt, A. Reiche, Scale-up of microfiltration processes, Chem. Ing. Tech. 92 (2020) 746–758.
[77] A. Torres-Pinto, M.J. Sampaio, J. Teixo, C.G. Silva, J.L. Faria, A.M.T. Silva, Photo-Fenton degradation assisted by in situ generation of hydrogen peroxide using a carbon nitride photocatalyst, J. Water Process Eng. 37 (2020), 101467.
[78] C. Liu, Y. Zhang, F. Dong, X. Du, H. Huang, Easily and synchronously ameliorating charge separation and band energy level in porous g-C3N4 for boosting photooxidation and photoreduction ability, J. Phys. Chem. C. 120 (2016) 10381–10389.
[79] A. Torres-Pinto, H. Boumeriame, C.G. Silva, J.L. Faria, A.M.T. Silva, Boosting carbon nitride photoactivity by metal-free functionalization for selective H2O2 synthesis under visible light, ACS Sustain. Chem. Eng. 11 (2023) 894–909.
[80] M.J. Lima, A.M.T. Silva, C.G. Silva, J.L. Faria, Graphitic carbon nitride modified by thermal, chemical and mechanical processes as metal-free photocatalyst for the selective synthesis of benzaldehyde from benzyl alcohol, J. Catal. 353 (2017) 44–53.
[81] J.C. Lopes, M.J. Sampaio, R.A. Fernandes, M.J. Lima, J.L. Faria, C.G. Silva, Outstanding response of carbon nitride photocatalysts for selective synthesis of aldehydes under UV-LED irradiation, Catal. Today 357 (2020) 32–38.
[82] H. Wang, Y. Su, H. Zhao, H. Yu, S. Chen, Y. Zhang, X. Quan, Photocatalytic oxidation of aqueous ammonia using atomic single layer graphitic-C3N4, Environ. Sci. Technol. 48 (2014) 11984–11990.
[83] J. Wang, M. Li, S. Zhou, A. Xue, Y. Zhang, Y. Zhao, J. Zhong, Controllable construction of polymer/inorganic interface for poly(vinyl alcohol)/graphitic carbon nitride hybrid pervaporation membranes, Chem. Eng. Sci. 181 (2018) 237–250.
[84] M.A. Barros, M.J. Sampaio, A.R. Ribeiro, C.G. Silva, A.M.T. Silva, J.L. Faria, Interactions of pharmaceutical compounds in water matrices under visible-driven photocatalysis, J. Environ. Chem. Eng. 9 (2021), 104747.
[85] R.A. Fernandes, M.J. Sampaio, G. Dražić, J.L. Faria, C.G. Silva, Efficient removal of parabens from real water matrices by a metal-free carbon nitride photocatalyst, Sci. Total Environ. 716 (2020), 135346.
[86] L. Xu, L. Li, L. Yu, J.C. Yu, Efficient generation of singlet oxygen on modified g-C3N4 photocatalyst for preferential oxidation of targeted organic pollutants, Chem. Eng. J. 431 (2022), 134241.
[87] Y. Li, M. Gu, M. Zhang, X. Zhang, K. Lv, Y. Liu, W. Ho, F. Dong, C3N4 with engineered three coordinated (N3C) nitrogen vacancy boosts the production of 1O2 for Efficient and stable NO photo-oxidation, Chem. Eng. J. 389 (2020), 124421.
[88] A.R. Lado Ribeiro, N.F.F. Moreira, G. Li Puma, A.M.T. Silva, Impact of water matrix on the removal of micropollutants by advanced oxidation technologies, Chem. Eng. J. 363 (2019) 155–173.
[89] M. Peñas-Garzón, M.J. Sampaio, Y.L. Wang, J. Bedia, J.J. Rodriguez, C. Belver, C. G. Silva, J.L. Faria, Solar photocatalytic degradation of parabens using UiO-66-NH2, Sep. Purif. Technol. 286 (2022), 120467.
[90] S. Leong, A. Razmjou, K. Wang, K. Hapgood, X. Zhang, H. Wang, TiO2 based photocatalytic membranes: a review, J. Membr. Sci. 472 (2014) 167–184.
[91] D. Li, Z. Feng, B. Zhou, H. Chen, R. Yuan, Impact of water matrices on oxidation effects and mechanisms of pharmaceuticals by ultraviolet-based advanced oxidation technologies: a review, Sci. Total Environ. 844 (2022), 157162.
[92] L. Madhura, S. Kanchi, M.I. Sabela, S. Singh, K. Bisetty, Inamuddin, Membrane technology for water purification, Environ. Chem. Lett. 16 (2018) 343–365.